



Impact of Canard on the Flowfield over the Wing in Various Flow Regimes

A. R. Davari^{1*}, M. R. Soltani²

¹ Department of Engineering, Science and Research Branch, Islamic Azad University, Tehran, Iran

² Department of Aerospace Engineering, Sharif University of Technology, Tehran, Iran

ABSTRACT: An in-depth study has been undertaken to investigate the vortical flow pattern on a generic canard-wing configuration at the Mach numbers 0.1, 0.8, and 2.0. The results show that the downwash flowfield due to canard decreases the effective angle of attack seen by the front half of the wing by at least 3% or more, which postpones the vortex formation and development. The rear half especially at the outboard section on the other hand is dominated by the canard upwash field, giving rise to the effective angle of attack to at least 5% of the original value. The interaction of the canard vortex with the wing leading edge vortex has been observed to increase the vortex strength and size on the wing. The present results have found a nearly 10% increase in vortex size due to canard-wing vortices interaction. In supersonic flow due to the impact of the oblique shocks and the consequent pressure rise, the primary flow separation to form the leading edge vortex and the vortex break down onsets were shown to occur at higher angles of attack, when compared to those in the transonic regime. The present results could be employed to design and optimization of canard and wing in certain types of aircraft and missiles to enhance maneuverability and operational performance.

Review History:

Received: Jun. 20, 2021

Revised: Aug. 27, 2021

Accepted: Oct. 09, 2021

Available Online: Oct. 14, 2021

Keywords:

Vortex burst

Vortex core

Induced angle of attack

Canard

Sweep

1- Introduction

The canard-wing configurations in modern aircraft for maintaining air superiority have long been a topic of interest in aerodynamic design. Usually, the main benefits of canards are realized when the aircraft is performing a maneuver. The flow interaction between canard and wing is one of the most important aspects of the close-coupled canards and still is a dark corner in the existing knowledge of aerodynamics.

The flowfield due to a canard, located very close to the wing, has a strong interaction with the flow over the wing and creates complicated interactions between two vortices, interactions between vortex and solid surface, and also a change in upwash and downwash flows resulting in a change in effective angle of attack. Enormous numerical and experimental studies have been devoted to such interactions in closely coupled canard-wing configurations.

The initial studies revealed that the best aerodynamic performance and the angle of attack, at which it occurs, can be remarkably enhanced by bringing a delta-shaped canard close to a delta wing [1]. The works performed by Gloss [2-4] shed light on the role of canard planform shape and its longitudinal and lateral locations on the aerodynamic behavior of a typical canard-wing-body combination. An extensive experimental study was performed by Hummel and Oelker [5, 6] which set out the interaction between canard and wing vortices. They visualized the vortex path and determined the effect of the canard vortex on the wing surface pressure.

*Corresponding author's email: ardavari@srbiau.ac.ir

Zhiyong [7] studied the effect of canard horizontal and vertical positions relative to the wing on vortex burst onset over the wing. Hayashibara et al. [8] examined a canard-wing configuration in a water tunnel using the dye flow visualization technique and studied the vortex breakdown position during the pitching motion of the canard. They pointed out that compared with an isolated wing, there is a delay in vortex breakdown for a canard-wing configuration. This time delay was found to be maximum when the canard is in close proximity to the wing.

Stark [9] has proposed an analytic method using linearized theory to calculate the unsteady aerodynamic forces on a canard configuration in supersonic flow, which has first been examined in the 1960s for the SAAB 37 Viggen, the first canard military airplane. This method was based on source singularity distribution on a subsonic leading edge. The approach and its associated mathematical treatments gave approximate results and were too restrictive to be extended.

In another survey, the influence of an oscillating canard on an X-31A-like model has been reported [10]. It has been worked out that if favorable interaction with the wing vortical flowfield during low pitch rates is achieved, the oscillating canard and the wing may adversely interact during high pitch rates. Also in general, small-amplitude pitching oscillations can adversely affect the wing vortical flowfield

Chen et al [11] examined a close-coupled coplanar canard configuration in unsteady pitching motion to study the role of canard in dynamic flow characteristics. They have reported



a transition phenomenon during the upstroke, in which the canard-wing vortices switched from a counter-rotating vortex to a co-rotating one. This is due to the effective angle of attack. In downstroke, the canard vortex shed strong downwash flow, which created a high pressure region on the suction side of the wing and lead to a loss of lift.

The computational studies have long been employed to investigate the aerodynamic superiorities of the closed coupled canard-wing configurations. Many of these numerical computations have been approved by the wind and water tunnels tests [12-15]. According to the results, the vortex breakdown over the wing in presence of a canard occurs farther from the wing trailing edge than that for an isolated wing.

The complicated vortex flows over delta wings have been the subject of several independent surveys. The international Vortex Flow Experiment program, VFE-1 has been commenced in 1984 to provide a database to support the numerical simulations at that time [16]. The advances in numerical schemes and hardware led to considerable prosperities in the development of fast and efficient numerical schemes and necessitated further experimental supports. This was the starting point for the VFE-2 program in 2001 [17].

It was found, during VFE2, that the vortex formation process strongly depends on Reynolds number. The outer primary vortex gets stronger and moves upstream as increasing the Reynolds number while the inner primary vortex is attenuated and moves towards the fuselage [18]. The Mach number increase from subsonic to transonic hastens the formation of the inner primary vortex and pushes it upstream and towards the body. The outer primary vortex strength decreases accordingly.

In recent surveys, it has been pointed out that the primary vortex core gets closer to the wing and extends on the surface as increasing the Mach number. It has also been found that the vertical clearance between the vortex core and the surface in subsonic flow is nearly constant while in supersonic flow, this height considerably decreases. Some recent numerical simulations have shown that the secondary vortex in supersonic high angle of attack flow occurs prior to the primary vortex [19].

Once the vortex structure is diminished, lift starts to decay. Thus, it is desirable for the vortex burst to be delayed as far as possible to get a higher lift. The canard induces a non-uniform distribution of local angles of attack on the wing surface, which leads to a non-conical vortex formation over the wing and delays the vortex breakdown to higher angles of attack [20]. On the other hand, the wing produces an upwash field on the canard which, increases its lift. The wing also induces a longitudinal velocity component on the canard. This induced velocity delays the vortex breakdown onset on the canard and increases its performance at moderate to high angles of attack [21, 22].

Despite valuable knowledge that has been achieved about the problem of canard-wing interaction, very limited works have been reported to devote to compare this interaction in various flow regimes. The surveys were mostly focused on

either supersonic or low subsonic flows and no attempts have already been made to relate the corresponding flowfields at various regimes. One reason is that the flow measurement in various flow regimes needs various equipment, including the model, the wind tunnel, the pressure sensors, and of course the proper mechanisms to change the model angle of attack and canard deflection angle. This is one of the most evident gaps in the existing knowledge of canard-wing aerodynamics.

Secondly, the previous investigations were mainly confined to the total force and moment measurement of the vehicle. The individual force on the wing in the absence of the contributions from the other components is one of the major factors in the aerodynamic design of canard and wing and their relative positions which can hardly be found in the available literature. However, note that a great deal of such investigation results are subjected to military classifications and limitations and are not publically available.

In this paper, some new aspects of the canard-wing interactions have been studied. Two models of closely coupled canard-wing attached to a semi-body have been tested in incompressible, transonic, and supersonic regimes to identify the role of the flow regime on canard-wing aerodynamic interaction. The experiments were performed individually at a low speed and also in a speed wind tunnel. There were some subtle differences in the geometric details of the models to adopt the wind tunnel systems. However, the main parameters including the wing and the canard sweep angles, aspect ratios, and the clearance between the two platforms were preserved.

2- The Models and the Experimental Apparatus

Two models have been manufactured, one for the low-speed incompressible regime and the other for high-speed transonic and supersonic flows. Both models were canard-wing-semi body configuration similar to those examined in previous studies [5, 6, 16, 17]. The canard could be removed from the body to examine the isolated wing as well. Both canard and wing in both models have 60° sweep angle.

The low speed tests were performed in a closed type subsonic wind tunnel having a test section of 80×80 cm². The maximum speed obtained in this tunnel is 100 m/sec and the present experiments have been performed at a free stream velocity of 60 m/sec corresponding to a Reynolds number of 1.11×10^6 . For the low speed model, 64 pressure taps were provided on the wing upper surface. Fig. 1 shows this model and the tubes connecting the taps to the pressure transducers.

The high speed tests were performed in a Tri-sonic suction-type wind tunnel having a test section dimensions of 60×60 cm². The maximum Mach number in this tunnel is 2.5 and the present experiments have been performed at two Mach numbers of 0.8 and 2.0. Two electric motors were exploited to control the model angle of attack and canard deflection angle, along with potentiometers to measure their values. Several high frequency Kullite-type pressure sensors have been placed inside the model to record the time-dependent pressures on the wing and the canard. Based on the test

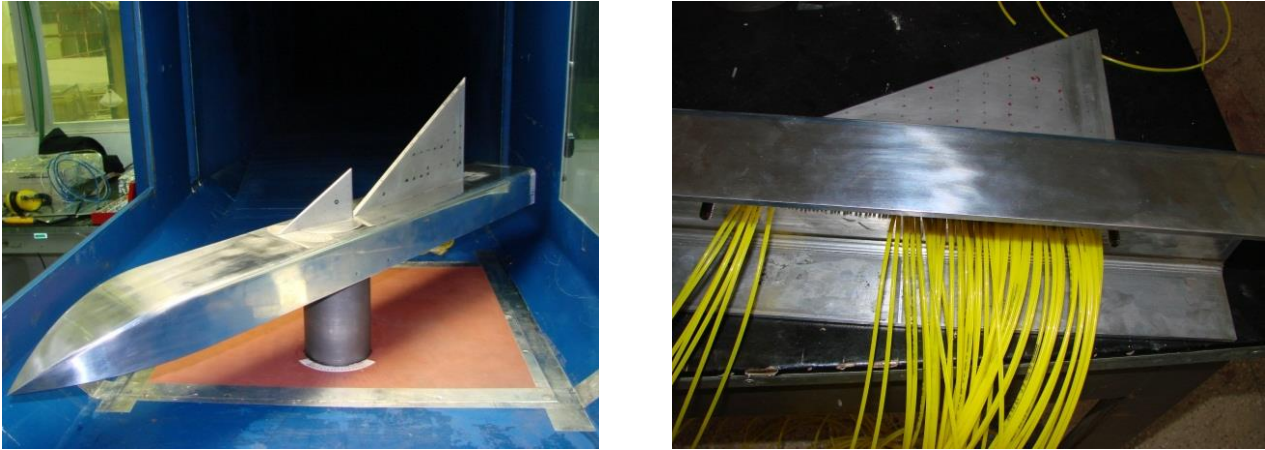


Fig. 1. The model for low speed tests

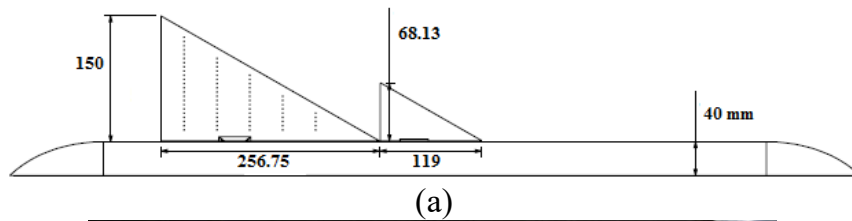


Fig. 2. The model for high speed tests, (a) the schematic view, (b) the model installed on the sidewall

section and the model dimensions, the maximum blockage ratios for the low speed and the high speed tests were 4.8 and 3.1, respectively.

The model for high speed tests is actually similar to the one constructed for the low speed incompressible experiments [23, 24] and is shown in Fig. 2. The thickness ratios for canard and wing were 0.158 and 0.058, respectively. Totally 69 pressure taps have been drilled on the wing for pressure measurements. The location of the taps on both low and high speeds models has been determined based on a numerical study on the model and has been arranged in such a way that the important regions on the wing could be captured.

For both experiments, a 64-channel A/D board along with digital filters and signal amplifiers were used to simultaneously acquire data from the pressure transducers and the potentiometers. The present experiments consist of pressure measurement on the wing, using the Kullite pressure transducers. The low-speed experiments were conducted at a Mach number of about 0.15 and the high-speed ones were at two Mach numbers of 0.8 and 2.0. In all experiments, the wing surface pressures have been measured for both canard-wing and isolated wing configurations.

To check the data repeatability and uncertainty, the incompressible tests were repeated 5 times and the high speed

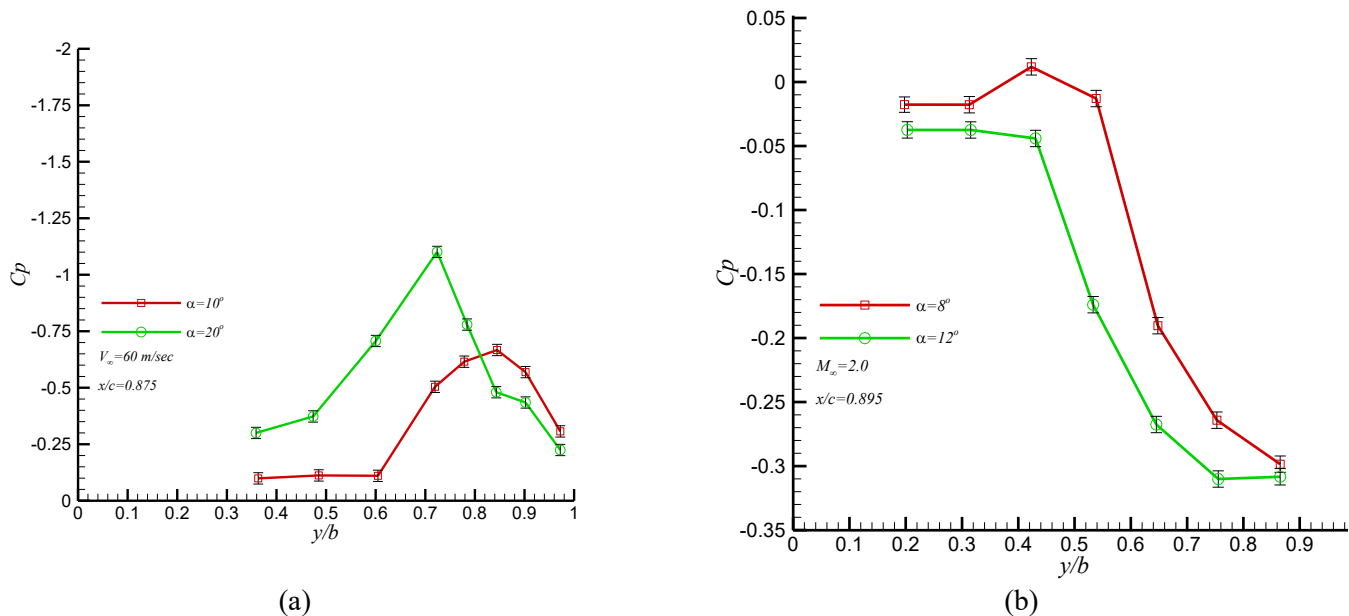


Fig. 3. The measurement uncertainties, (a) low speed tests, (b) supersonic tests

ones were repeated 3 times for some selected cases in the test matrix. Once the mean and the standard deviation of the data were determined, based on a 95% confidence level and using the t-student table in statistics, the maximum data uncertainty was calculated to be $\pm 4.02\%$ and $\pm 3.56\%$ for the low and high speed tests respectively. According to this analysis, Fig. 3 shows the error bars for two typical sets of data in low and high speed tests.

3- Results and Discussion

As noted earlier, both low speed incompressible and high speed experiments have been conducted. The canard-off runs were also performed to study the role of canard on the flow-field over the wing. The low-speed data are presented in this section followed by the high speed ones.

3- 1- Low-speed incompressible flow

Fig. 4 shows the sectional pressures at several angles of attack for both canard-wing and isolated wing configurations. The peaks in pressure are the signature of the leading edge vortex. On this basis, for the canard-wing configuration, the wing vortex tends toward the leading edge, whereas for the isolated wing the leading edge vortex is closer to the wing root.

For the canard-wing configuration up to moderate angles of attack, the suction peaks in the front regions of the wing are higher than those for the isolated wing whereas near the trailing edge, the magnitude of suction on the wing for the canard-wing case evidently reduces. This shows that the favorable effects of canard are primarily observed at the front half of the wing at moderate to high angles of attack.

Fig. 4 also elucidates that for the isolated wing configura-

tion at $\alpha = 20^\circ$, the vortex burst reaches the wing trailing edge, Fig. 4(a). This is in agreement with the water tunnel visualization tests for a delta wing of 60° sweep angle. At the angle of attack of 30° , the leading edge vortex over the isolated wing has nearly been broken down while for the wing in presence of canard, the vortex still exists and covers a comparatively large area on the wing.

Investigations also revealed that a canard induces a downwash velocity field next to its trailing edge and an upwash field out of its span. Consequently, the effective angle of attack of the wing reduces at the inner region, which in turn, postpones the flow separation in this area of the wing. In contrast, the effective angle of attack outboard of the wing increases as a result of the canard upwash field. This hastens the separation in this region and weakens the magnitude of suction on the wing. The net effect is to postpone the process of wing vortex formation as well as its breakdown in canard-wing configurations.

Since the effective angle of attack, seen by the wing leading edge differs along the span, the impact of the vorticity field on the isolated wing vortex is somehow different than that on the wing downstream of a canard. To sum up, the wing in a canard-wing configuration sees a smaller angle of attack than the isolated wing.

The surface pressure contours on the wing, shown in Fig. 5 present a better qualitative view of the surface flowfield. For the isolated wing at moderate to high angles of attack at which the vortex burst reaches the wing surface, the vortical flow due to the canard amplifies the low pressure region on the wing and extends it towards the trailing edge. As a result, the burst onset is postponed and the lift goes on its increasing behavior with the angle of attack.

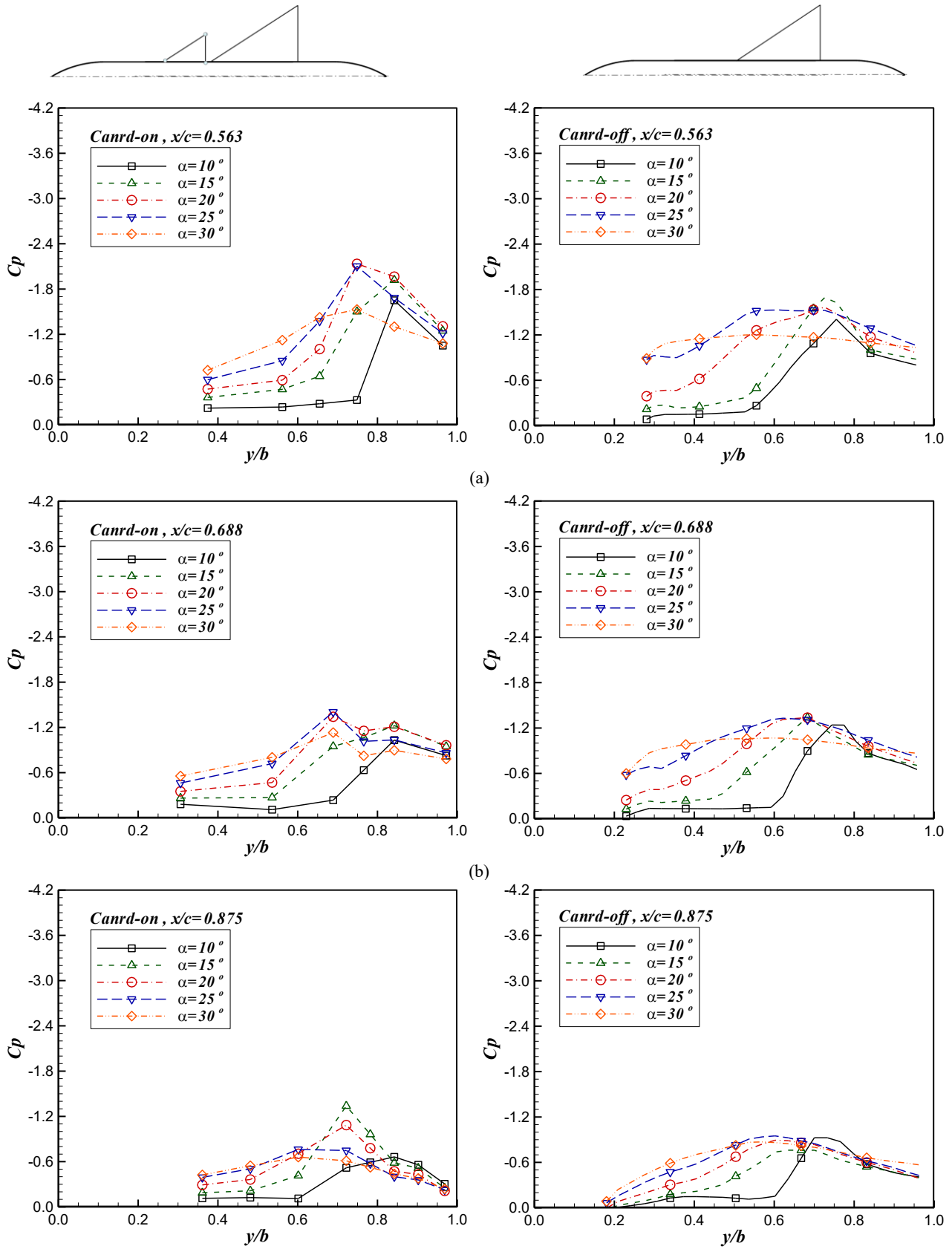


Fig. 4. The spanwise surface pressure on the wing in incompressible flow, (a) $x/c=0.563$, (b) $x/c=0.688$, (c) $x/c=0.875$.

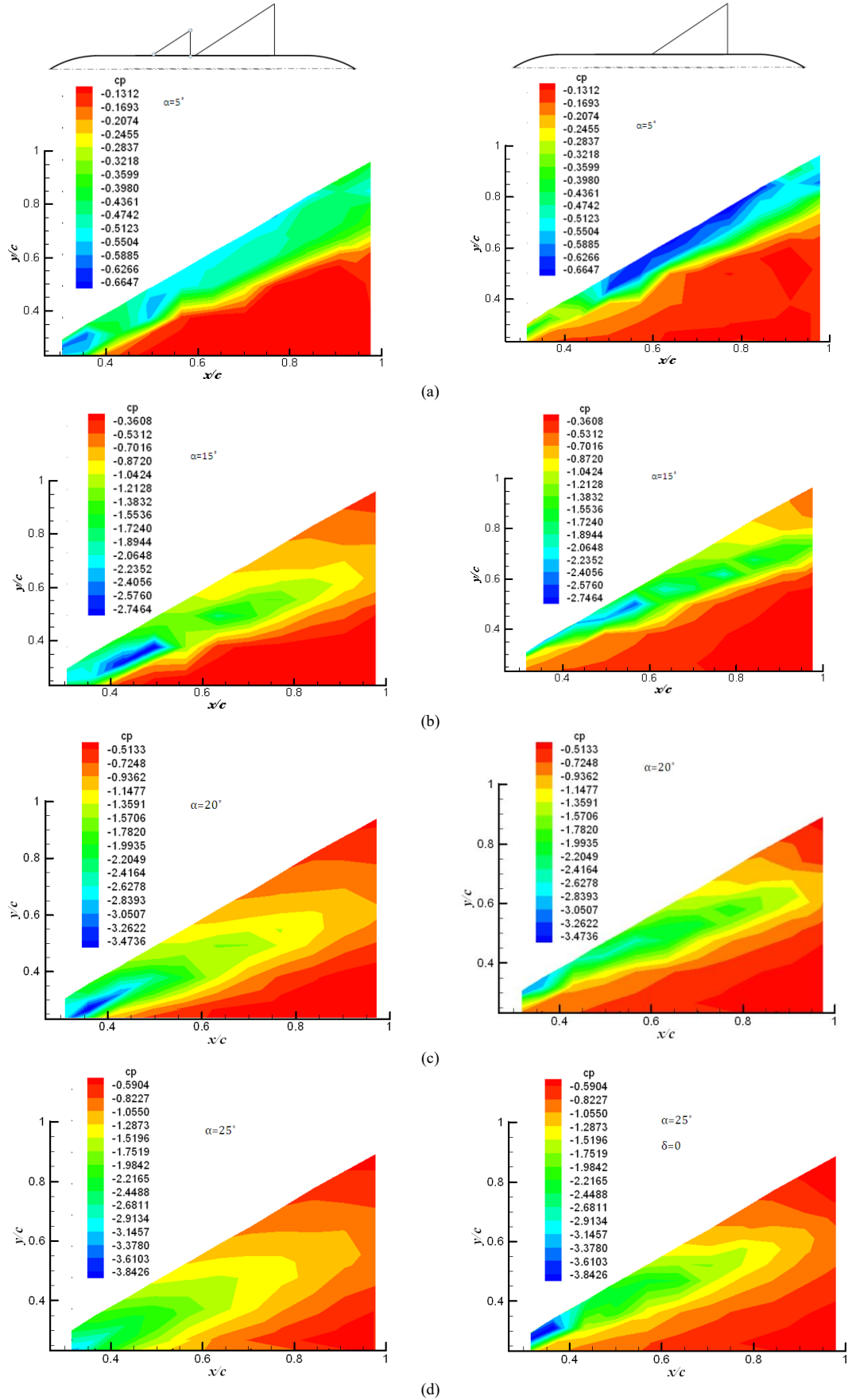


Fig. 5. The surface pressure contours on the wing in incompressible flow (a) $\alpha=5$, (b) $\alpha=15$, (c) $\alpha=20$, (d) $\alpha=25$, (e) $\alpha=30$. (Continued)

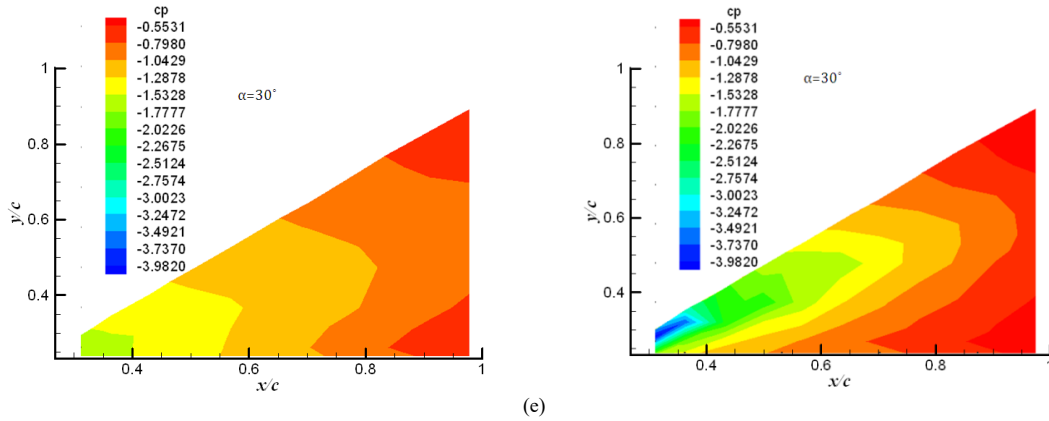


Fig. 5. The surface pressure contours on the wing in incompressible flow (a) $\alpha=5^\circ$, (b) $\alpha=15^\circ$, (c) $\alpha=20^\circ$, (d) $\alpha=25^\circ$, (e) $\alpha=30^\circ$

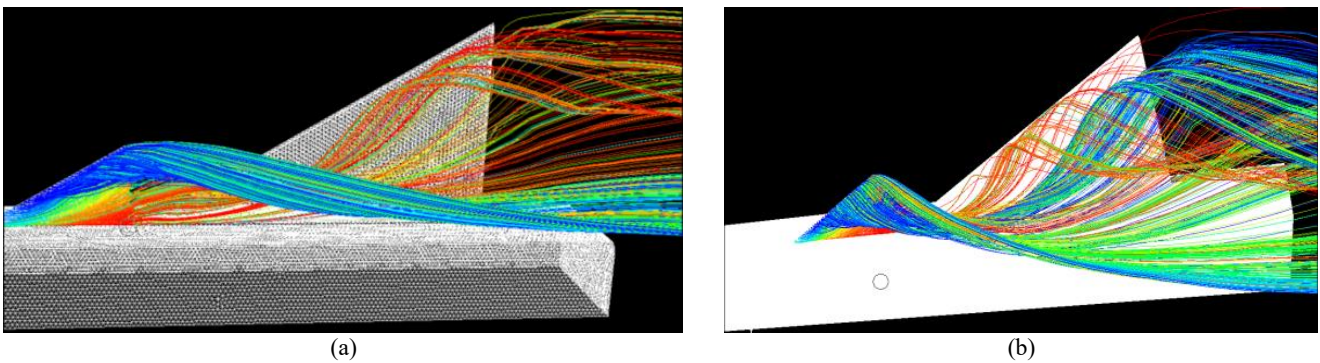


Fig. 6. The pathlines due to canard on the wing in incompressible flow, (a) $\alpha=15^\circ$, (b) $\alpha=25^\circ$ [25].

The numerical surveys on this configuration, performed by the authors using ANSYS-FLUENT, verified the above-mentioned discussions [25]. The results show that the vortex and the wake emanating from the canard extend downstream on the wing. These, along with the wing leading edge vortex are the dominant contributors to the canard-wing aerodynamic interaction. Fig. 6, taken from ref. [25], illustrates the canard pathlines on the wing. Details of the numerical solution have been set out in this reference. The vortical flow due to the canard proceeds towards the wing at its inboard area. The mild separated flow from canard, on the other hand, can be observed to be combined with the leading edge vortex of the wing.

The two types of flows due to the canard, namely the canard vortex and its wake, when combined with the wing vortex, make a very complex flowfield over the wing and

both the computational and experimental techniques should be employed to attack the problem of the aerodynamic interaction in canard-wing configurations.

Similar findings were also reported by Hummel and Oelker [5,6] shown in Fig. 7. According to their experimental analysis on a nearly similar canard-wing-body configuration using conical five-hole probe together with balance data and surface pressure measurements, they found that the canard induced upwash along the wing leading edge increases the effective angle of attack at that region. This increase in the angle of attack, which is the origin of the leading edge vortex formation, supports the leading edge flow separation, as well. Hummel's results also show that the canard vortex system under the wing influence moves above the wing towards the body and at the same time, downward towards the wing surface.

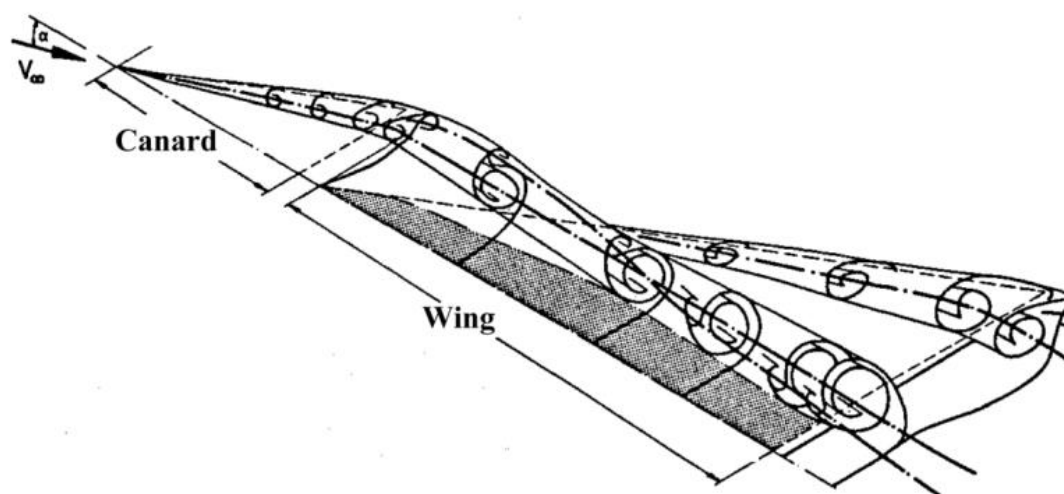


Fig. 7. The schematic structures of canard and wing vortices at low angles of attack [5].

3- 2- Compressible flow

The wing pressure distributions at various sections for both the isolated wing and the wing downstream of the canard have been shown in Fig. 8 for the transonic regime at $M=0.8$. The suction peaks can be observed for both configurations. On the isolated wing, the absolute values of the peaks are higher than those in presence of canard in the front regions, Figs. 8(a) and 8(b). However at the rear half, the absolute values of the pressure on the wing downstream of the canard increases. This shows that the effective angle of attack seen by the front area of the wing in presence of canard is less than that for the isolated wing, while at the rear half it is evidently higher.

From incompressible tests remind that the vortex covered a large portion of the isolated wing span near the trailing edge at $\alpha=20^\circ$ and when the canard was placed upstream, this region has been slightly stretched and increased in strength, Fig. 4. At $M=0.8$ for similar conditions, the vortex in presence of a canard covers a wider spanwise region on the wing and no particular pattern can be seen in the position of the vortex core. It seems that the domain of movement of the vortex core in the incompressible regime is wider than that for the compressible flow. According to flow similarity laws, the streamlines around the body at compressible flow are further apart from each other than in the incompressible regime. It is likely that the vortex in an incompressible flow is more affected by the changes in pressure and vorticity along the streamline in the outer layers and would have more freedom to move while at $M=0.8$, a nearly stationary vortex has been pointed out.

As noted earlier, the vortex burst on an isolated 60° swept wing is supposed to occur near the trailing edge at about $\alpha=20^\circ$ and the canard downwash postpones it to higher an-

gles of attack. However, at $M=0.8$, the vortex on the isolated wing at $\alpha=20^\circ$ seems to start breaking down near the trailing edge. Despite having been boosted up by the canard flow, the spanwise pressure distribution near the trailing edge, Fig. 8(c) suggests that the breakdown onset on the wing surface at $M=0.8$ is hastened by the compressibility effects.

A numerical survey has also been performed on the same isolated wing at high speed regimes for both static and oscillatory pitching cases [19, 26]. Fig. 9 compares the numerical and experimental values for pressure coefficient at $M=0.8$, $\alpha=12^\circ$, and at two chordwise sections, $x/c=0.3$ and $x/c=0.7$. Note that these two sections were just presented to be compared with the numerical simulations. However, the other sections, i.e. $x/c=0.443$, 0.594 , and 0.895 contained a clearer representation of the flow phenomena and have thus been presented in other places in this paper.

A fairly good agreement is observed between the numerical and experimental results, especially in predicting the vortex core location over the wing. However, the suction peak measured in the present experiments was slightly higher than those predicted by the numerical simulations. This might be attributed to the free stream uniformity, turbulence intensity, and the roughness effects in the experiments and of course, the turbulence modeling and the mesh generated within the boundary layer in numerical simulations.

For supersonic flow, $M=2.0$, the pressure distributions are shown in Fig. 10. The wing vortex is stretched and lies closer to the surface at $M=2.0$ compared to the corresponding former cases at $M=0.8$ and $M=0.15$, which is the signature of the oblique shock waves emanating from the wing and the canard leading edges. The latter has also caused the absolute values of the surface pressure at $M=2.0$ to be generally higher than those at $M=0.8$.

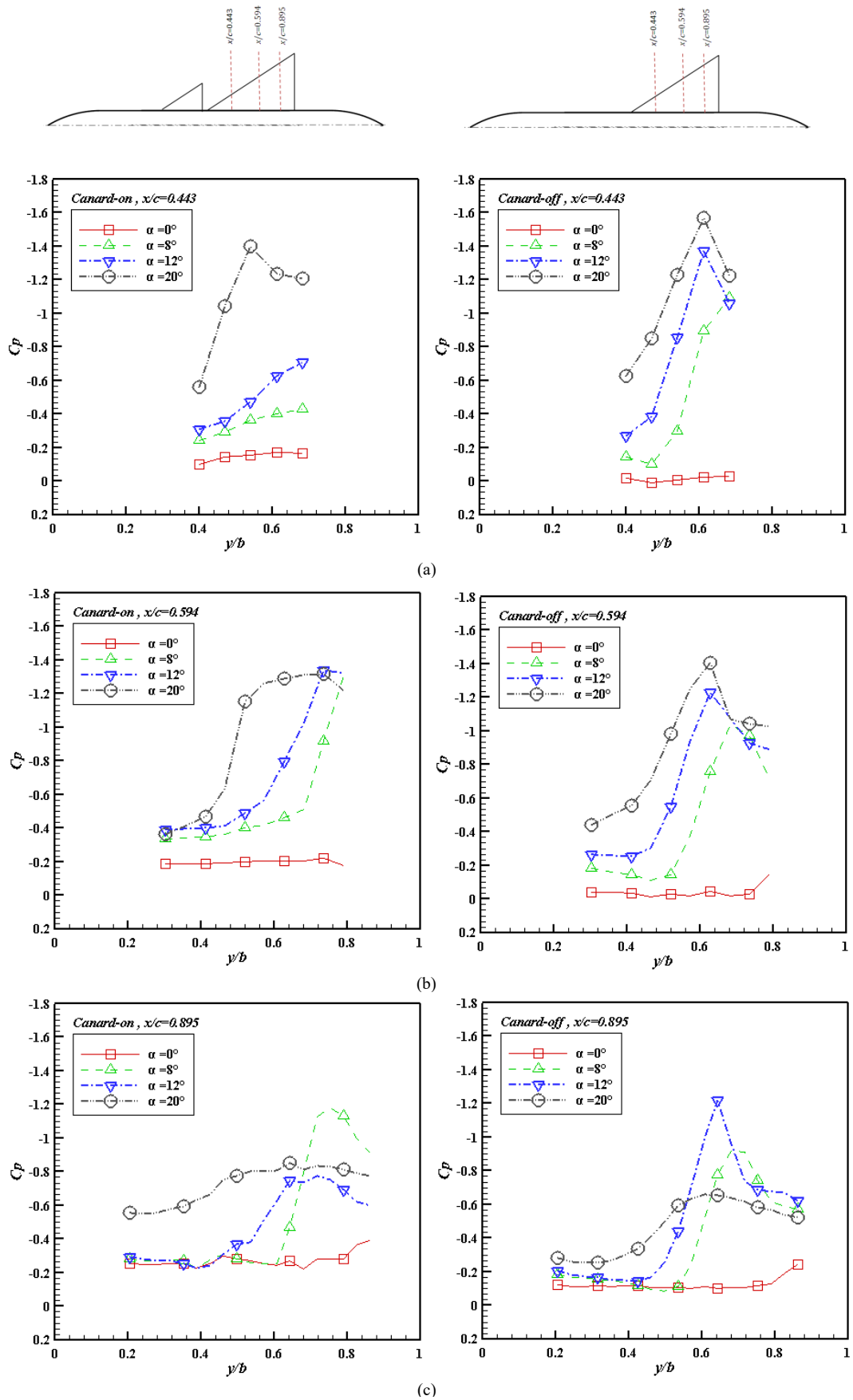


Fig. 8. The spanwise surface pressure on the wing at $M=0.8$, (a) $x/c=0.443$, (b) $x/c=0.594$. (c) $x/c=0.895$

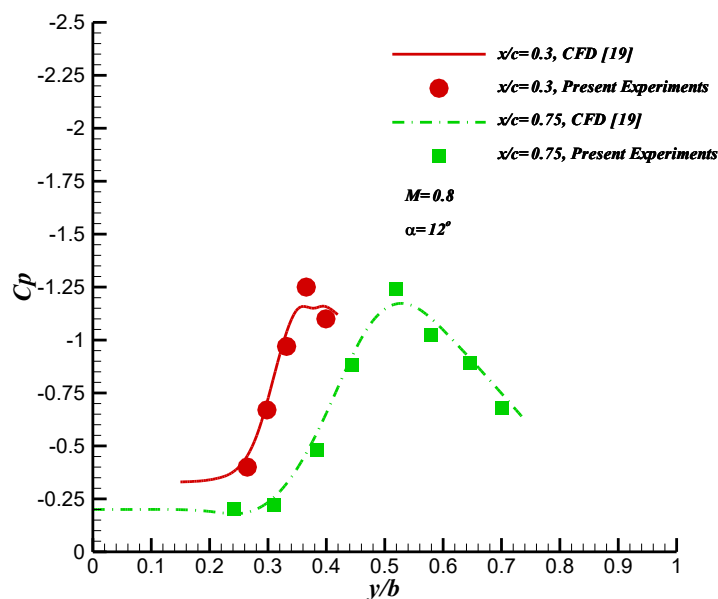


Fig. 9. Comparison with the numerical results at $M=0.8$

From Fig. 10(a) for $x/c=0.433$ and at moderate angles of attack, stronger suction peaks and more developed vortex regions can be observed on the isolated wing compared to the wing in presence of canard. As a result of the canard downwash field and its impact on the front and middle areas of the wing, the effective angle of attack has been reduced and the vortex formation and development have been postponed to higher angles of attack. Note also that the vortex lies closer to the leading edge on the wing surface in presence of the canard.

For $M=2.0$ and at $\alpha=20^\circ$, in contrast to $M=0.8$, no evidence of flow separation to form the vortex is observed in the canard-wing configuration and just a rotational region can be identified in the vicinity of the wing leading edge. This suggests that for the canard-wing configuration, the vortex roll-up position has been moved downstream as the Mach number was increased from $M=0.8$ to $M=2.0$. Fig. 10(b) also approves this lag in vortex formation at $x/c=0.594$ at $M=2.0$ in comparison to $M=0.8$, for the angles of attack higher than 12° . However, for the isolated wing at $\alpha > 12^\circ$, the suction peak has been developed and the signature of the secondary vortex can be observed, Fig. 10(c). The vortex tends to move inboard towards the fuselage and its strength increases as moving downstream on the wing in the absence of a canard.

At $x/c=0.895$ shown in Fig. 10(c), for $\alpha > 8^\circ$ the vortex strength on the wing downstream of canard is evidently less than that on the isolated wing and is situated closer to the fuselage. At $\alpha=20^\circ$, the suction peak on the isolated wing diminishes while the vortex on the wing downstream of the canard is still active and has been increased in both strength and size. In this section, the secondary vortex can still be observed on the isolated wing, while for the canard-wing the

vortex is fully developed with a small decrease in its strength, as observed earlier, the favorable effect of canard fades off at the rear sections of the wing.

To sum up, the wing vortex for both configurations has been lifted off from the surface towards the oblique shock as the angle of attack increases at $M=2.0$ compared to $M=0.8$. Also, the flow separation and vortex formation at the front area of the wing downstream of the canard is postponed to higher angles of attack as the flow Mach number increases from 0.8 to 2.0. For the wing in presence of a canard, two vortices are dominated on the wing surface. The canard vortex amplifies the wing's one which merges downstream at $x/c=0.895$, forming a stronger vortex.

At the rear half, the wing surface in the canard-wing configuration is exposed to a stronger suction field than that in the absence of canard. Note that the wing surface pressure in a canard-wing arrangement is affected by two successive oblique shocks emanating from canard and wing leading edges while for an isolated wing, there exists a single stronger shock ahead of the wing. The lower suction on the wing in the canard-wing configuration compared to the isolated wing at the front half can thus be deemed to be due to the canard downwash field. The rear half region on the wing is more dominated by the oblique shock and the wing downstream of the canard, experiences a stronger suction than the isolated wing. The increase in pressure for the flow passing through a single oblique shock emanating from the wing vertex is higher than that when the flow passes through two tandem shocks from both the canard and the wing leading edges. In a supersonic flow, this may also be responsible for the stronger suction at the rear half of the wing downstream of the canard.

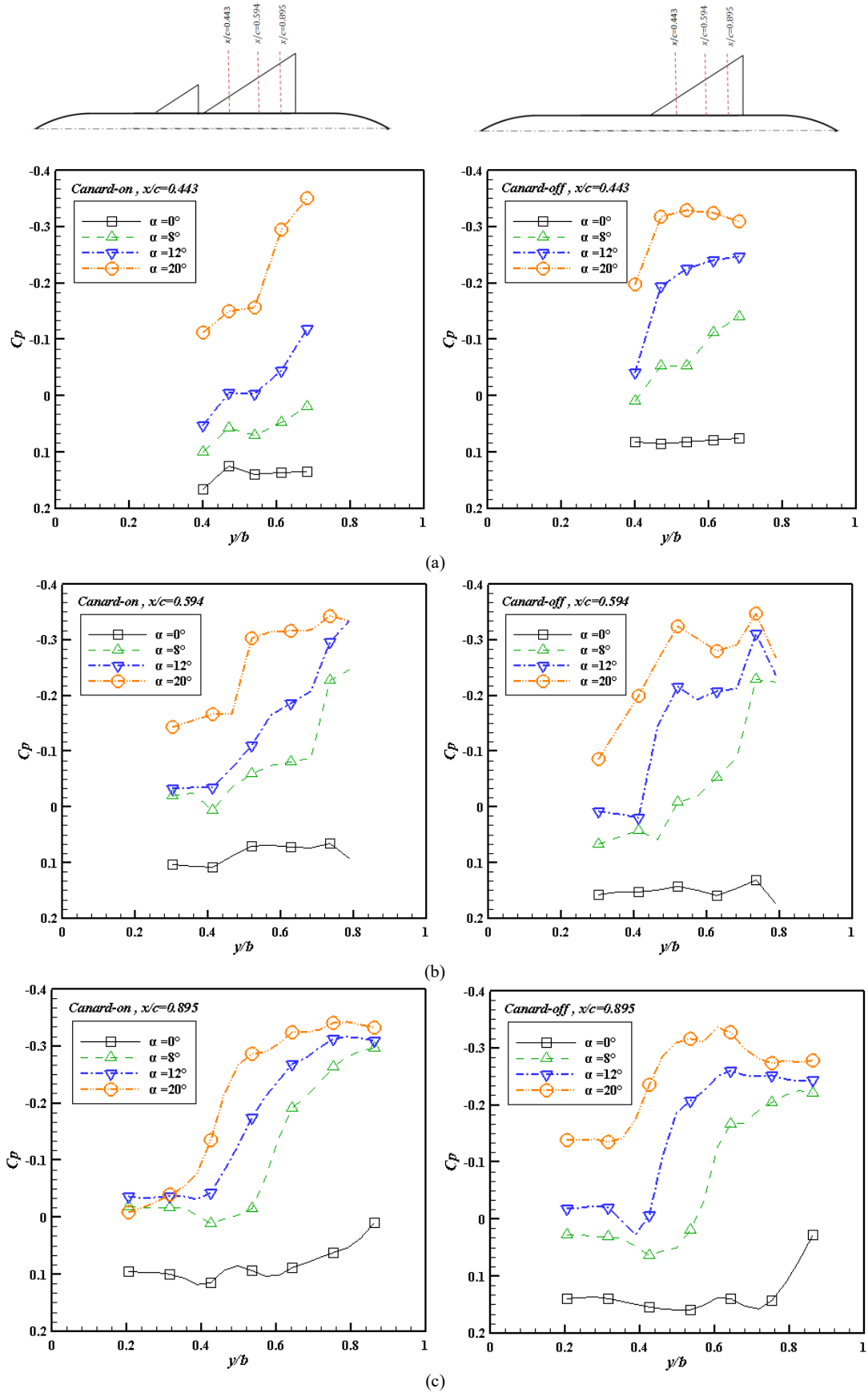


Fig. 10. The spanwise surface pressure on the wing at $M=2.0$, (a) $x/c=0.443$, (b) $x/c=0.594$. (c) $x/c=0.895$.

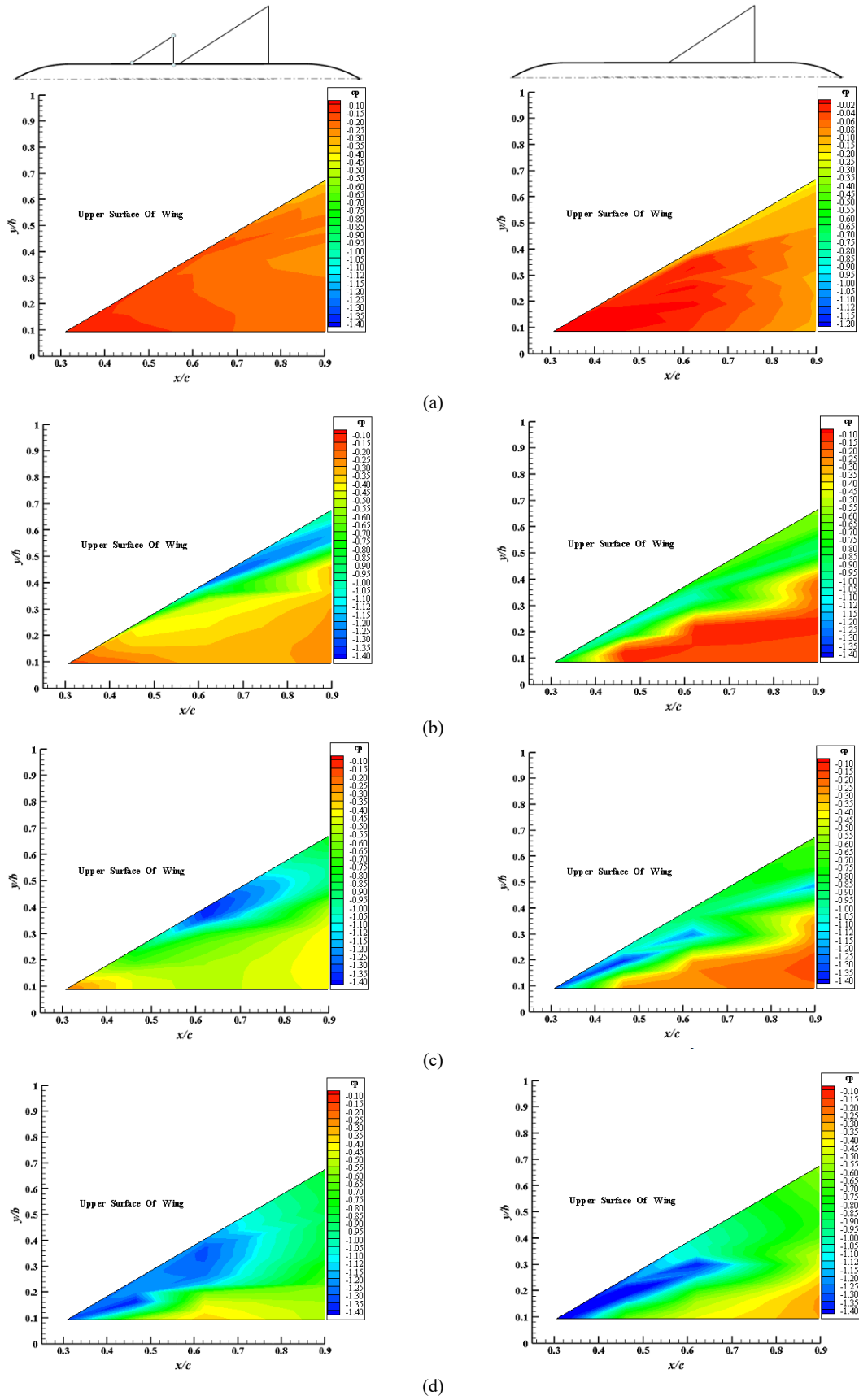


Fig. 11. The surface pressure contours on the wing at M=0.8, (a) $\alpha=0$ (b) $\alpha=8$, (c) $\alpha=12$, (d) $\alpha=20$

Shown in Fig. 11 are the pressure contours on the isolated wing and the wing downstream of the canard, respectively at $M=0.8$. According to Fig. 11, the vortex formation for the isolated wing starts at the front region of the wing at the angles of attack larger than about 12° , where a weak small vortex is observed in Fig. 11(b). This weak vortex grows in size and strength as increasing the angle of attack. At $\alpha=20^\circ$, shown in Fig. 11(c), the vortex strength and size have been increased.

For the canard-wing configuration, at $\alpha=8^\circ$ the leading edge vortex has been formed, while for the wing alone at the same angle of attack, the vortex signature is hardly identified. Further, note that the vortex on the wing alone tends to move inboard as increasing the angle of attack whereas the vortex on the wing in presence of a canard, moves outboard towards the leading edge. This evidently shows the role of canard on the flowfield induced over the wing. The vortex size on the wing in presence of canard has been increased at higher angles of attack due to the canard-wing vortices interaction and the result would be a single stronger vortex on the wing downstream of the canard compared to the isolated wing.

Similar flow patterns were observed in the contours of local Mach number in numerical simulations for the same isolated wing [26], shown in Fig. 12, at the free stream Mach number of 0.8, $x/c=0.3$, and at the three angles of attack examined in Fig. 11. The low-pressure signature of the vortex can be detected in Fig. 11, where the experimental pressure distributions have been presented.

At $\alpha=8^\circ$, the secondary flow separation can be seen beside the primary vortex, which can be observed as a region of low

pressure streak in Fig. 11. As the angle of attack increases, the primary vortex becomes larger in both size and strength. Returning back to Fig. 11, the low pressure region is more prominent at the front half. At $\alpha=20^\circ$, the local Mach number has reached about two times the free stream value. The numerical results [26] have revealed that the vortex break down position, in this case, has been reached to about $x/c=0.6$, which can also be pointed out in surface pressure contour in the present experiments shown in Fig. 11(d).

Fig. 13 shows the pressure contours at $M=2.0$ on the wing alone and that in presence of canard. The vortex formation has been started from $\alpha=8^\circ$. As pointed out previously, the increases in surface pressure at $M=2.0$ compared to $M=0.8$ is due to the oblique shocks emanating from the wing and canard vertices. The leading edge vortex in the canard-wing configuration is stronger and lies closer to the leading edge. As increasing the angle of attack, the low pressure region on the wing downstream of the canard extends and approaches the leading edge, while for the isolated wing, this low pressure region tends to move inboard towards the fuselage.

For $M=0.8$ at $\alpha=20^\circ$, the leading edge vortex over the wing can be detected at the front regions near the wing apex, while at $M=2.0$, the vortex on the wing appears far from the apex. This is also evidence for the oblique shock at the wing apex which has postponed vortex formation to downstream locations. As a consequence of the oblique shock ahead of the wing leading edge at $M=2.0$, the low pressure region on the wing has been stretched on the surface and extended towards the fuselage.

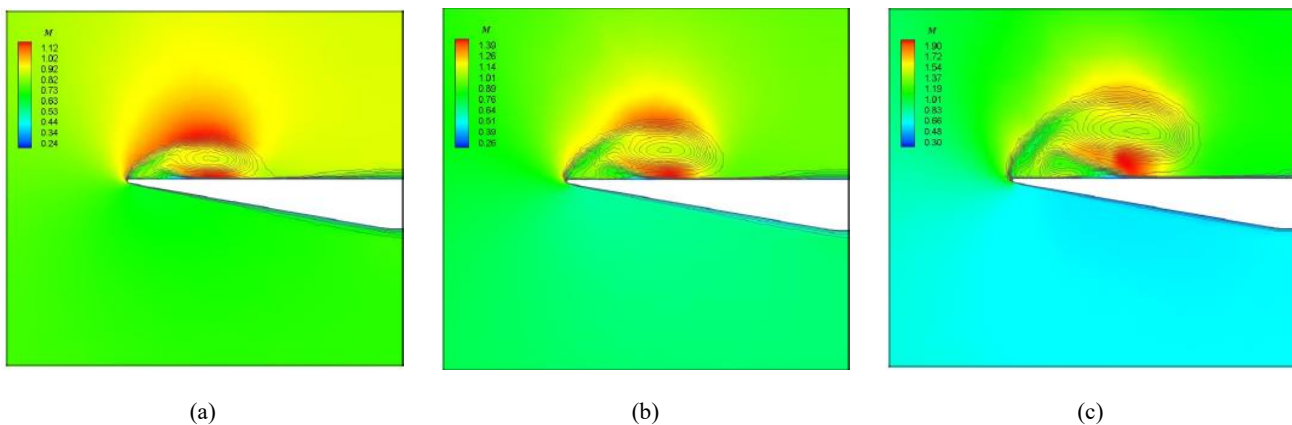


Fig. 12. The contours of Mach number from the numerical simulations at $M=0.8$ and $x/c=0.3$ on the isolated wing, (a) $\alpha=8^\circ$, (b) $\alpha=12^\circ$, (c) $\alpha=20^\circ$ [26]

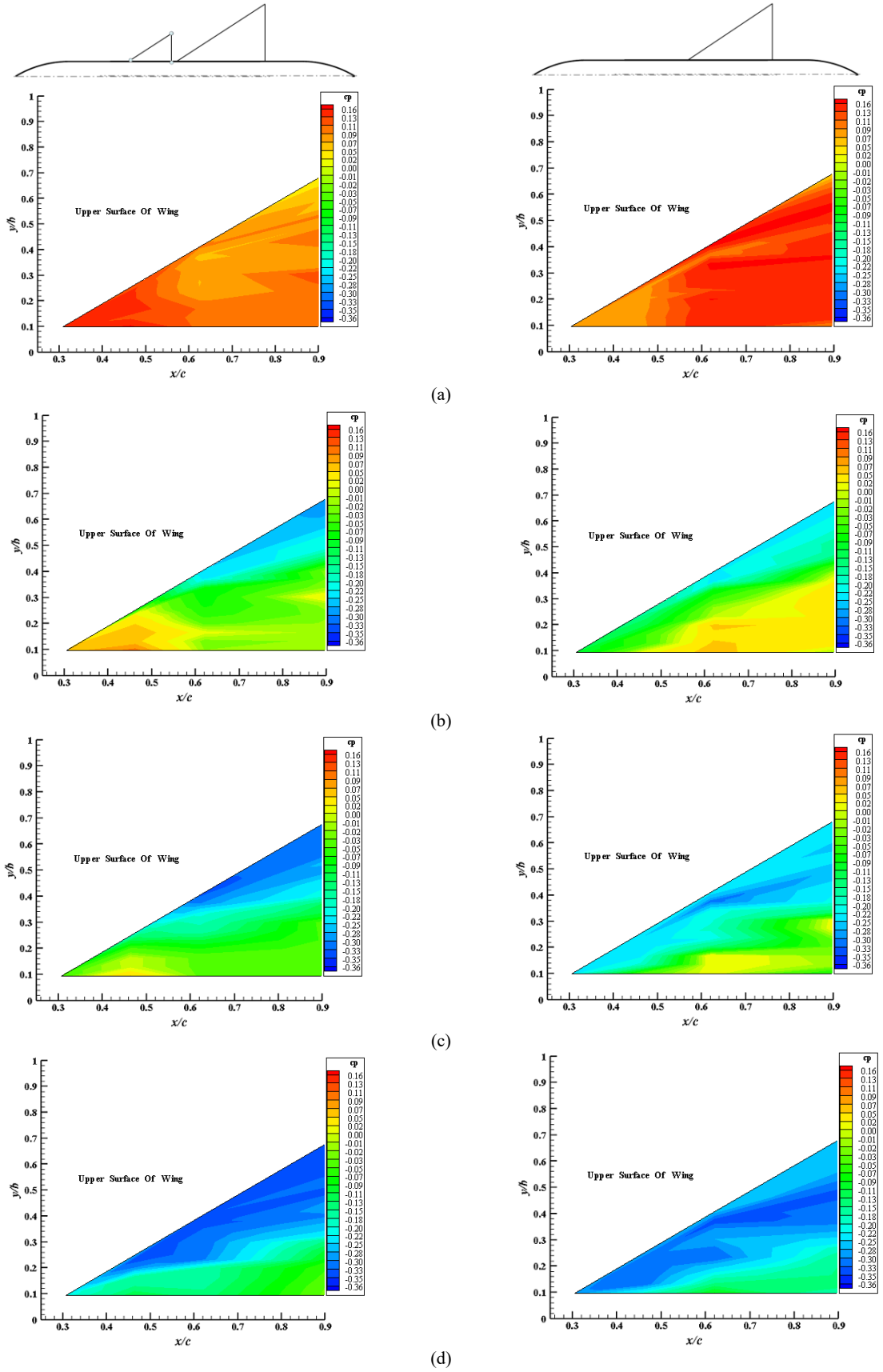


Fig. 13. The surface pressure contours on the wing at $M=2.0$, (a) $\alpha=0$, (b) $\alpha=8$, (c) $\alpha=12$, (d) $\alpha=20$.

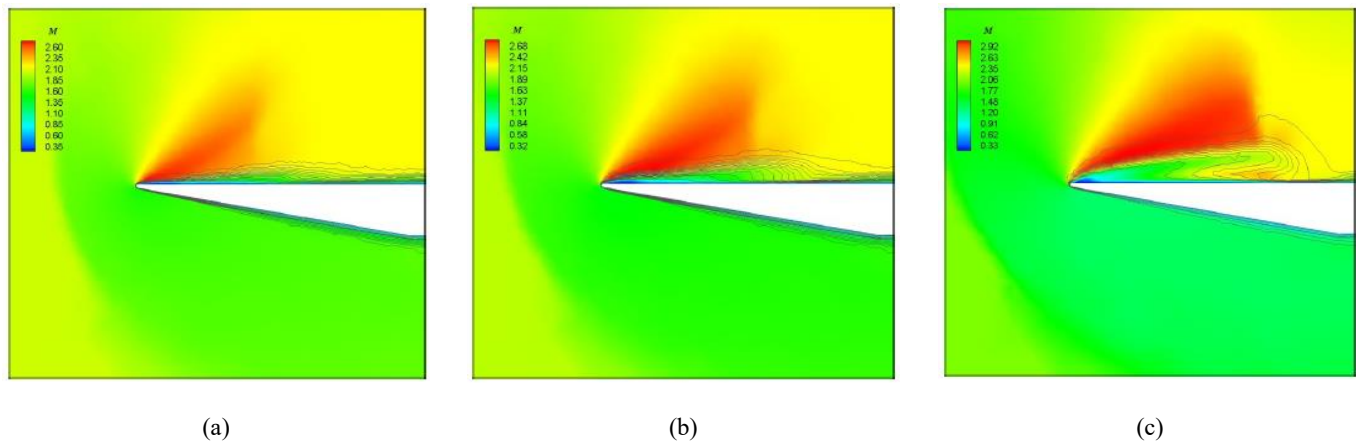


Fig. 14. The contours of Mach number from the numerical simulations at $M=2.0$ and $x/c=0.3$ on the isolated wing, (a) $\alpha=8^\circ$, (b) $\alpha=12^\circ$, (c) $\alpha=20^\circ$ [26]

The contours of local Mach number in numerical simulations for the isolated wing [19, 26] are shown in Fig. 14, at the free stream Mach number of 2.0, $x/c=0.3$, and at the three angles of attack examined in Fig. 13. At $\alpha=8^\circ$, a separation bubble downstream of the normal shock is evident. The bubble size increases at higher angles of attack. At $\alpha=20^\circ$, the flow separation reaches the leading edge, which is confirmed by the pressure contours in the present experiments shown in Fig. 13(d). This flow pattern is characterized by a separated vortex from the leading edge accompanied by an oblique shock next to that. Note that the shock wave squeezes the vortex at high angles of attack. The wider low pressure region in the surface pressure contour from the present experiments, Fig. 13, approves this phenomenon.

4- Conclusion

Extensive wind tunnel tests have been performed on a canard-wing-body and wing-body configurations at incompressible, transonic and supersonic flow regimes to study the role of canard on the flowfield over the wing. In both transonic and supersonic regimes, the downwash flowfield due to canard decreases the effective angle of attack seen by the front half of the wing, which postpones the vortex formation and development. The rear half especially at the outboard section near the leading edge, on the other hand, is dominated by the canard upwash field, giving rise to the effective angle of attack. The non-uniform induced angle of attack on the wing has been shown to postpone the vortex growth and break down on the canard-wing configuration. The interaction of the canard vortex with the wing leading edge vortex has been observed to amplify the suction peaks and increase the vortex size on the wing. In supersonic flow due to the impact of the oblique shocks and the associated high-pressure field, the primary flow separation to form the leading edge vortex in the front region and the vortex break down in the rear half on the wing were shown to occur at higher angles of attack comparing to those in the transonic regime. The shock waves in supersonic flow push the wing vortex towards the surface and as increasing the angle of attack, the vortex lifts off from

the surface. In supersonic flow, the wing vortex reaches the wing tip at a higher angle of attack compared to the subsonic flow with a higher suction peak.

References

- [1] J. Zhang, J. Lei, J. Niu, Numerical investigation of aerodynamic characteristics of free-spinning tail projectile with canards roll control, Proceedings of the Institution of Mechanical Engineers, Part G: Journal of Aerospace Engineering, 235(6) (2021) 687-702.
- [2] B.B. Gloss, L.W. Mckinney, Canard-wing lift interference related to maneuvering aircraft at subsonic speeds, (1973).
- [3] B.B. Gloss, The effect of canard leading edge sweep and dihedral angle on the longitudinal and lateral aerodynamic characteristic of a close-coupled canard-wing configuration, (1974).
- [4] B.B. Gloss, Effect of Canard Location and Size on Canard-Wing Interference and Aerodynamic-Center Shift Related to Maneuvering Aircraft at Transonic Speeds. NASA Report, 1974, NASA TN D-7505, (1974).
- [5] H.-C. Oelker, D. Hummel, Investigations on the vorticity sheets of a close-coupled delta-canard configuration, Journal of aircraft, 26(7) (1989) 657-666.
- [6] D. Hummel, H.C. Oelker, Effects of canard position on the aerodynamic characteristics of a close-coupled canard configuration at low speed, Zeitschrift für Flugwissenschaften und Weltraumforschung, 15(2) (1991) 74-88.
- [7] Z. Lu, Z. Lu, A study on flow patterns and aerodynamic characteristics for canard-double delta wing configuration, in: 35th Aerospace Sciences Meeting and Exhibit, 1994, pp. 324.
- [8] S. Hayashibara, R. Myose, L. Miller, The effect of a 70 swept canard-on the leading edge vortices of a 70 swept delta wing during dynamic pitching, AIAA Paper 97, 613 (1997).
- [9] V.J. Stark, Canard-wing interaction in unsteady

- supersonic flow, *Journal of aircraft*, 26(10) (1989) 951-952.
- [10] S.K. Hebbbar, M.F. Platzer, D.-M. Liu, Effect of canard oscillations on an X-31A-like model in pitching maneuver, *Journal of aircraft*, 32(5) (1995) 1157-1160.
- [11] Q. Chen, T. Hu, P. Liu, Q. Qu, H. Guo, R.A. Akkermans, The dynamic vortical flow behaviour on a coplanar canard configuration during large-amplitude-pitching, *Aerospace Science and Technology*, 112 (2021) 106553.
- [12] S.M. Hitzel, R. Osterhuber, Enhanced maneuverability of a delta-canard combat aircraft by vortex flow control, *Journal of Aircraft*, 55(3) (2018) 1090-1102.
- [13] J. Sahu, F. Fresconi, Computational and Experimental Free-Flight Motion of a Subsonic Canard-Controlled Body, in: 35th AIAA Applied Aerodynamics Conference, 2017, pp. 3400.
- [14] S.B. Wibowo, S. Sutrisno, T.A. Rohmat, Computational study of flow interactions over a close coupled canard-wing on fighter, *International Journal of Aviation, Aeronautics, and Aerospace*, 6(1) (2019) 5.
- [15] K.V.R.A.N.K.P.B.S.T. Sudhakar Uppalapati, CFD Analysis on Eurofighter Typhoon at Canard, *International Journal of Advanced Science and Technology*, 29(9s) (2020) 2408 - 2415.
- [16] D. Hummel, G. Redeker, A new vortex flow experiment for computer code validation, NATO RESEARCH AND TECHNOLOGY ORGANIZATION NEUILLY-SUR-SEINE (FRANCE), 2003.
- [17] D.J. Hummel, The international vortex flow experiment 2 (VFE-2): background, objectives and organization, *Aerospace science and technology*, 24(1) (2013) 1-9.
- [18] J.M. Luckring, D. Hummel, What was learned from the new VFE-2 experiments, *Aerospace Science and Technology*, 24(1) (2013) 77-88.
- [19] M. Hadidoolabi, H. Ansarian, Computational investigation of vortex structure and breakdown over a delta wing at supersonic pitching maneuver, *Journal of the Brazilian Society of Mechanical Sciences and Engineering*, 40(2) (2018) 1-17.
- [20] S.B. Wibowo, B. Basuki, T.A. Rohmat, S. Siswantoro, F. Nugroho, P. Ginting, Z. Anwar, *Vortex Dynamics Study and Flow Visualization on Aircraft Model with Different Canard Configurations*, *Fluids*, 6(4) (2021) 144.
- [21] Y. Dong, Z. Shi, K. Chen, J. Chen, Experimental investigation of the effects of sideslip on canard-configuration aircraft at high angle of attack, *AIP Advances*, 9(5) (2019) 055114.
- [22] Z. Ali, W. Kuntjoro, W. Wisnoe, I. Ishak, M. Katon, N. Ahmad, Aerodynamics Analysis on the Effect of Canard Aspect Ratio on Blended Wing Body Aircraft using CFD Simulation, in: IOP Conference Series: Materials Science and Engineering, IOP Publishing, 2020, pp. 012015.
- [23] M. Soltani, F. Askari, A. Davari, A. Nayebedeh, Effects of canard position on wing surface pressure, (2010).
- [24] M.H. Doolabi and M.A. Rabbani, Numerical investigation of the flowfield over a closely coupled canard-wing configuration in subsonic flow. The 26th annual conference of the Iranian Society of Mechanical Engineers (ISME 2018), Semnan University, Iran 24-26 April, (2018).
- [25] A.R. Davari, M.H. Doolabi, M. Soltani, M. Izadkhah, Aspects of canard-wing vortices interaction in subsonic flow, *Scientia Iranica*, 22(3) (2015) 743-754.
- [26] M. Hadidoolabi, H. Ansarian, Computational Investigation of Vortex Breakdown over a Pitching Delta Wing at Supersonic Speeds, *Scientia Iranica*, 24(6) (2017) 2915-2928.

Nomenclature

x	Longitudinal position from wing apex
y	Spanwise position from wing root
c	Wing chord length at the root
b	Wing span measured from the root
C_p	Local pressure coefficient, referenced to the free stream pressure
M	Free stream Mach number
α	Angle of attack
Re	Free stream Reynolds number based on the wing root chord

HOW TO CITE THIS ARTICLE

A. R. Davari, M. R. Soltani, *Impact of Canard on the Flowfield over the Wing in Various Flow Regimes*, *AUT J. Mech Eng.*, 6 (1) (2022) 113-128.

DOI: [10.22060/ajme.2021.20189.5993](https://doi.org/10.22060/ajme.2021.20189.5993)

